Surface Science 602 (2008) 2604–2609

Contents lists available at ScienceDirect

Surface Science

journal homepage: www.elsevier.com/locate/susc

Density functional theory study of Ni/Ni_3Al interface alloying with Re and Ru

Cong Wang [a,*], Chong-Yu Wang [a,b]

[a] Department of Physics, Tsinghua University, Beijing 100084, PR China
[b] The International Center for Materials Physics, Chinese Academy of Sciences, Shenyang 110016, PR China

ARTICLE INFO

Article history:
Received 4 May 2008
Accepted for publication 17 June 2008
Available online 28 June 2008

Keywords:
Density functional calculations
Alloys
Metal–metal interfaces

ABSTRACT

The optimal geometries and mechanical properties of (001) Ni/Ni_3Al interface alloying with Re and Ru are studied using density functional theory. By placing alloying elements on cleavage or slip interface planes, brittle cleavage and generalized stacking fault energies are calculated for (001) interface. Simulated results indicate that the preferred slip direction is ⟨110⟩ in (001) plane. Re and Ru atoms preferred to substitute Al site of γ' phase. Both of doping Re and Ru enhance the coherent strength of interface, and additions of Re are more effective in strengthening interface compared with Ru. Based on the criteria for ductile behavior, our results show that Re and Ru are good candidates for improving ductility of γ/γ' superalloy.

1. Introduction

γ-Ni, which has a face-centered cubic (*fcc*) structure (with a lattice constant of 3.524 Å), is used as a major component of many alloys for high-temperature applications [1] for its good oxidation resistance and excellent ductility [2]. The intermetallic compound γ'-Ni_3Al is of great interest for its attractive applications in the aerospace and power industries as a high-temperature structural material, and it exhibits an ordered *fcc* $L1_2$ structure (with the lattice constant of 3.570 Å). γ'-Ni_3Al in bulk or thin-film state has unique properties such as low density, high strength at elevated temperatures [3]. Although ductility and even low-temperature superplasticity of specially processed Ni_3Al alloys have been reported recently [4–6], the practical use of the intermetallics is still severely restricted by its room-temperature brittleness and poor high-temperature creep resistance. Odette et al. [7] and Heathcote et al.'s works [8] reinforce the brittle intermetallic matrix with ductile refractory metals to increase the ductility. Ni and Ni_3Al have not only similar structures but also close lattice constants (the misfit of γ/γ' is below 1.3%). In this context, combining Ni and Ni_3Al could produce grain-to-grain epitaxial interfaces – Ni based single crystal (SC) superalloy. Unfortunately, the poor ductility and brittle grain-boundary fracture still limits the applications of single crystal superalloy. Creep rupture strength of SC superalloys were reported to be improved by adding W, Re and Ta [9]. Recently, a fourth generation of SC superalloys with Ru as a new alloying addition has been under development [10]. Generally, the fourth generation SC superalloys contain the elements of W, Cr, Co, Mo, Re, Ru, Ta, Ti, etc. [11]. Ta, Al and Ti partition to the interdendritic region [12], during solidification. W and Re are reported to partition to the dendrite core [12], which will lead to the formation of topologically close-packed (TCP) phases [13], and causes considerable degradation of the mechanical properties. Recent experiment [14] showed that the TCP phases could be eliminated through the addition of Ru. Among many experimental and theoretical works, the addition of Re and Ru were reported to improve the mechanical properties of Ni-base SC superalloys. However, to date, investigations on Ru-containing Ni-base superalloys have been conducted over a relatively narrow range of composition. Also, little is known about their tendency to promote or reduce grain defect formation during single-crystal solidification. Meanwhile, the occupancy site of Re and Ru in Ni-base SC superalloys is still under discussion [15,16].

Brittle or ductile materials could be distinguished by their properties under mechanical loading: brittle materials break suddenly when they suffer small strains, while ductile materials deform plastically under large strains. At atomic scale, two competing processes are used to describe brittle and ductile behaviors of solid materials: (i) opening a crack; (ii) emitting dislocations at the crack tip [17,18]. Within the concept of ideal brittle cleavage, process (i) is modeled by the loss of bonding energy in the manner of cleavage decohesion [19–21]; process (ii), in the shearing displacement of atomic planes, the maximum energy associated with this progress decides the resistance of the dislocation emission [18], and the value of this energy is determined by the maximum value of the generalized stacking fault energy [22]. We aim to investigate the effect of doping ternary elements in cleavage and slip planes, and competing processes described above will be influenced. We could select classical molecular dynamics method to investigate progress (i) and (ii). This method has the advantage of fast and less computation cost, but it is less reliable and could not treat doping effect

* Corresponding author.
E-mail address: wangcong00@mails.tsinghua.edu.cn (C. Wang).

0039-6028/$ - see front matter © 2008 Elsevier B.V. All rights reserved.
doi:10.1016/j.susc.2008.06.017

due to the inherent approximations. On the other hand, first-principle calculations demand much more computational cost, such studies are published for $MoSi_2$ [23], and NiAl [24]. And both of the works focus on bulk properties, Medvedeva et al.'s work [25] provided study on the interfacial strength of NiAl/Mo interface. Our investigation concentrates on interface systems.

In this paper, we use density functional theory approach to investigate mechanical properties of Ni/Ni_3Al superalloy doped with Re and Ru at low temperatures. The rest of this paper is organized as follows: to view the detailed information of our models and methods see Section 2. By doping Re and Ru, the properties of cleavage are influenced. Discussions are provided in Section 3. The generalized stacking fault energies are obtained from the models of slipping planes(see Section 4). Both of the two progress are then compared for the possibility of improving ductility. In Section 5, we get a conclusion.

2. Model and methods

In this paper, total-energy calculations are performed within the framework of density functional theory, which is implemented in the planewave-based Vienna ab initio simulation package VASP [26,27]. In all of the calculations, the Perdew–Wang 91 exchange-correlation functional [28] within the generalized gradient approximation (GGA) is taken into account, a plane-wave cutoff energy of 500.0 eV for all the models, and the electron-ion interaction potential described by the projector augmented wave method [29] are used. The k points are set to be $16 \times 16 \times 16$ for bulks and $6 \times 6 \times 1$ for interfaces. The equilibrium geometries are determined by relaxation until all the forces less than 0.04 eV/Å. The thickness of vacuum layer is 12.00 Å. The reliability of our approach is demonstrated by the excellent agreement between calculated and experimental lattice parameters and bulk modulus, as listed in Table 1.

We model (001) γ/γ' interfaces with a repeated slab construction with three-dimensional translational symmetry. The sketch of our model is shown in Fig. 1. Fig. 2 illustrates the stacking sequence of the [001] orientated Ni_3Al bulk. The atomic structure of Ni bulk is the same with Ni_3Al bulk. Two series of models are considered in our calculations for (001) γ/γ' interfaces. One is hollow site model, and the other is top site model. Two models investigated in our calculations are labeled in Fig. 3a and b, respectively. In present work, each model contains 96 atoms.

Brittle cleavage formation was modeled by separating interface. Ideal brittleness was modeled with no atomic positions relaxed during cleaving. The generalized stacking fault energies as a function of the displacement $\boldsymbol{u}$ were calculated by shifting the γ' part relative to the fixed γ part. The atomic positions were fully relaxed in [001] direction, while fixed in the other directions to minimize tensile stress [34]. The volume of the supercell is kept constant, in order to keep a well-defined conditions to investigate the interactions of interfaces. The error introduced by the volume relaxation is small when compared to the atomic position relaxations [35].

Table 1
The calculated lattice constant a_0 and bulk modulus B_0

	Ni		Ni_3Al	
	a_0 (Å)	B_0 (GPa)	a_0 (Å)	B_0 (GPa)
Our results	3.526	196.8	3.570	180.8
Other DFT results [30]	3.540	191.6	3.564	182.4
EAM results [31]	3.520	181.0	3.571	N/A
Experiment [32,33]	3.520	181.0	3.570	240.0

Other DFT, EAM (embedded atom method) calculated results and experiment results are listed for comparison.

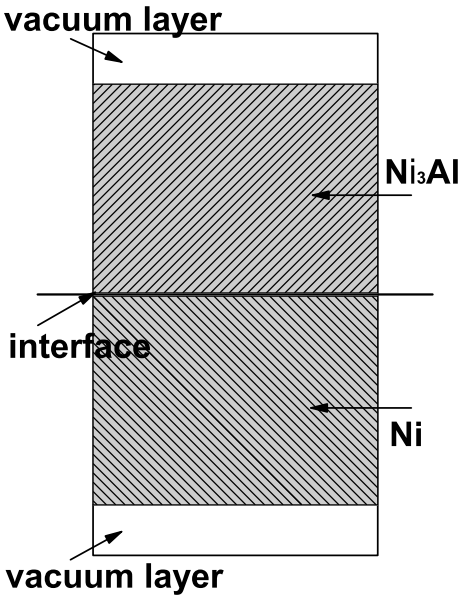

Fig. 1. The sketch of the calculated models.

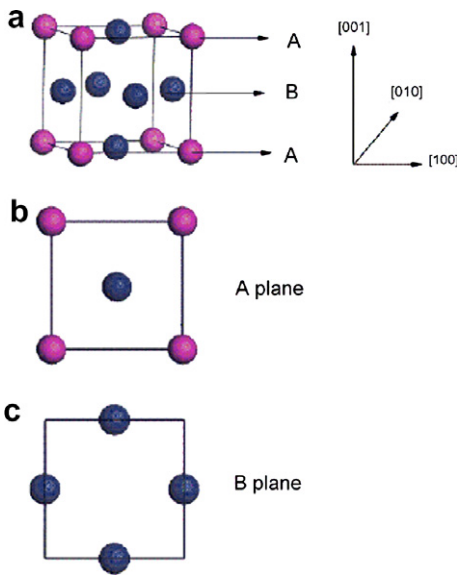

Fig. 2. Ni_3Al bulk orientated [001] direction. The purple ball denotes Al atom, and the blue ball denotes Ni atom. (a) Perfect Ni_3Al bulk with the stacking sequence (ABABAB.....); (b) atomic structure of A plane; (c) atomic structure of B plane. (For interpretation of the references to colour in this figure legend, the reader is referred to the web version of this article.)

In the present paper, two doping elements X=Re, Ru are considered. The substitute positions are: γ-Ni, γ'-Al, γ'-Ni. The atomic structures of the interface planes are sketched in Fig. 4. We consider the substitutions at the interface, because the dopants at the interface could strongly influence the cleavage and slip properties. The dopant interface coverage is 25%, and 1.04% concentration by volume in our calculations.

3. The effect of doping on the cleavage properties

The formation energy of interface E_f, which could be defined as follows:

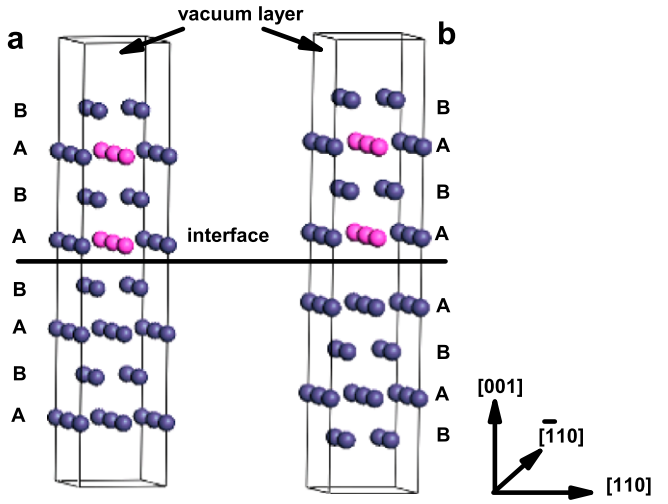

Fig. 3. The geometry of γ/γ' interface model. The purple ball denotes Al atom, and the blue ball denotes Ni atom. (a) The hollow site (001) interface model, Ni and Al atoms in γ' phase placed in the hollow site of Ni atoms in γ phase. ([001]:γ:ABAB.....AB|interface|[001]:γ':ABAB.....AB) stacking; (b) the top site (001) interface model, Ni and Al atoms in γ' phase placed directly on top site of Ni atoms in γ phase. ([001]:γ:BABA.....BA|interface|[001]: γ':ABAB.....AB) stacking. (For interpretation of the references to colour in this figure legend, the reader is referred to the web version of this article.)

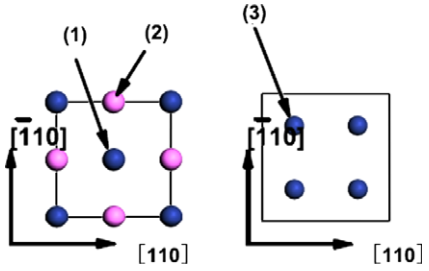

Fig. 4. The atomic structure of the interface plane. The purple ball denotes Al atom, and the blue ball denotes Ni atom. (1) The γ'-Ni substitution; (2) the γ'-Al substitution; (3) the γ-Ni substitution. (For interpretation of the references to colour in this figure legend, the reader is referred to the web version of this article.)

$$E_f = (E_{\gamma/\gamma'} - E_{\text{bulk-}\gamma} - E_{\text{bulk-}\gamma'})/A_i - (E_\gamma + E_{\gamma'}), \quad (1)$$

$$E_\gamma = (E_{\text{slab-}\gamma} - E_{\text{bulk-}\gamma})/A_{\text{s-}\gamma}, \quad (2)$$

$$E_{\gamma'} = (E_{\text{slab-}\gamma'} - E_{\text{bulk-}\gamma'})/A_{\text{s-}\gamma'}, \quad (3)$$

where $E_{\gamma/\gamma'}$ is the total energy of γ/γ' interface system, and A_i is the interface area. E_{bulk} is the total energy of bulk. E_{slab} is the total energy of a fully relaxed slab. $A_{\text{s-}}\gamma$ and $A_{\text{s-}\gamma'}$ are the area of each slab. $E\gamma$ and $E_{\gamma'}$ are surface formation energies of slabs. Interface formation energy can be viewed as the work required to create the interface from bulk materials. Convergency of the formation energies was tested. The formation energy of hollow site model is -4.15 J/m^2, while it is -2.31 J/m^2 for the top site model. This suggest that, the hollow site model is more energetic stable than the top site model. Thus only hollow site models are investigated in present work.

Griffith energy balance is widely used to describe the ideal brittle cleavage. When a solid material is separated into two blocks, the process accompanies the release of bonding energy. when propagating the crack, if mechanical energy release rate G is larger than the cleavage energy G_c, the material cleavages. Bonding energy release rate $G(x)$ depends on interface separation. Cleavage energy G_c is defined as $G_c = \lim_{x\to\infty} G(x)$. Usually, the cleavage energy per unit area G_c/A is more widely used. E_0 is the total energy of interface system in ground state. x is interface separation. And the definition of $G(x)$ is:

$$G(x) = E(x) - E(0). \quad (4)$$

We use calculated total energies at a series of fixed separations x_i to determine the cleavage energy G_c. We simulated the ideal cleavage, with no atomic relaxations. The $G(x_i)$ are fitted to the universal binding energy relation (UBER) [36]:

$$G(x) = G_c\left[1 - \left(1 + \frac{x}{l}\right)\exp\left(-\frac{x}{l}\right)\right]. \quad (5)$$

The stress is defined as:

$$\sigma(x) = \mathrm{d}G(x)/\mathrm{d}x. \quad (6)$$

The parameter l is defined by the maximum stress $\sigma_c = \max \sigma(x) = \sigma(x = l)$. The G_c and l usually depend on the orientation of cleavage plane. σ_c stands for the maximum tensile stress perpendicular to the given cleavage plane.

The bonding energies are listed in Table 2. The results indicate that both of Re and Ru can enhance the stability of γ/γ' interface system, and alloying with Re is more energetically stable than Ru. Among the three substitutions, γ'-Al substitution is the most energetically stable of all, and our results agree well with experiment work [15]. Fig. 5 shows that UBER fits very well with the calculated data. The results of fitted UBER are listed in Table 3. For pure interface, cleavage energy per area G_c/A is 4.36 J/m^2, the maximum stress $\sigma_c = 27.69$ GPa, and the relative interface separation l is 0.58 Å. From the results listed in Table 2, we know doping with Re and Ru could enhance the coherent energy of the γ/γ' interface. But not all of the substitutions could improve the mechanical properties of γ/γ' interface. $\text{Re}^{\gamma\text{-(Ni)}}$, $\text{Ru}^{\gamma\text{-(Ni)}}$, and $\text{Ru}^{\gamma'\text{-(Ni)}}$ substitutions reduce the cleavage energy per area by 0.08, 0.07 and 0.02 J/m^2. While, $\text{Re}^{\gamma'\text{-(Al)}}$, $\text{Re}^{\gamma'\text{-(Ni)}}$, and $\text{Ru}^{\gamma'\text{-(Al)}}$ substitutions increase the cleavage energy per area by 1.19, 0.53, and 0.82 J/m^2. The most stabilizing $\text{Re}^{\gamma'\text{-(Al)}}$ alloying could increase G_c/A by 27.3% compared with pure interface. From function (5) and (6), we give the stress as a function of interface separation x as follows:

$$\sigma(x) = G_c \times \left[\frac{x \times \exp\left(-\frac{x}{l}\right)}{l^2}\right]. \quad (7)$$

The trend of stress with x is plotted in Fig. 6. The maximum stress σ_c is increased by doping Re and Ru. From the results listed in Table 3, $\text{Re}^{\gamma'\text{-(Al)}}$ substitution is the most favored. It increase σ_c by 25.6%. From Fig. 6, the maximum stress exists at the same interface separation $x \approx 0.58$ Å. The parameter l does not change much after alloying.

4. The effect of doping on the slip properties

On atomic scale, the competitions between brittleness and ductility take place at the crack tip, where the tensile stress is enhanced by the crack tip [37]. The competition progresses of brittleness and ductility are the propagation of the crack by splitting the interface into two pieces and the emission of a dislocation, which blunt the crack and produce shielding stress. In the progress of propagating a crack, the energy required for an incremental advance in the crack front is $G(x)$. $G(x)$ is the energy release rate, x is the interface separation. When $x \to \infty, G(\infty) = G_c$. In order to nucleate a dislocation with Burgers vector $\boldsymbol{b}$, it is necessary to overcome

Table 2
The bonding energy E_b (ev) of alloying with Re and Ru

X^{site}	$\text{Re}^{\gamma\text{-(Ni)}}$	$\text{Re}^{\gamma'\text{-(Al)}}$	$\text{Re}^{\gamma'\text{-(Ni)}}$	$\text{Ru}^{\gamma\text{-(Ni)}}$	$\text{Ru}^{\gamma'\text{-(Al)}}$	$\text{Ru}^{\gamma'\text{-(Ni)}}$
E_b	−6.72	−7.70	−5.79	−3.53	−3.96	−3.26

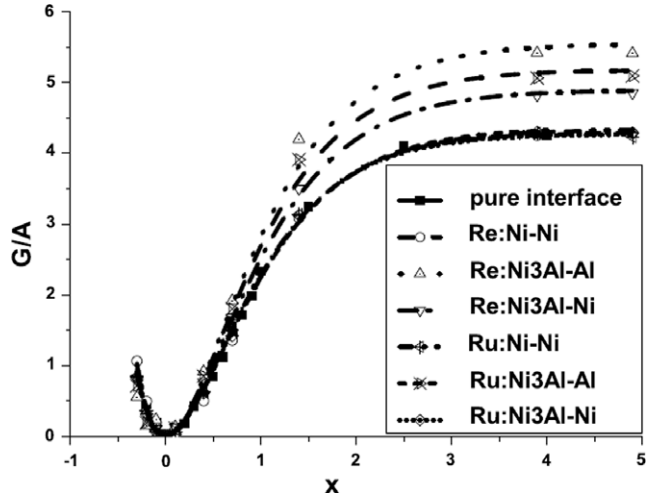

Fig. 5. The calculated cleavage energy release rate per unit area $G(x)/A$ in (J/m^2) verse the interface separation x(Å) for substitutions Re and Ru at γ-Ni,γ′-Al and γ′-Ni sites. The curves are obtained by fitting the calculated energies to UBER.

Table 3
The fitted UBER parameters for the pure γ/γ′ interface and doped interface

X^{site}	G_c/A	σ_c/A	l	$\Delta G_c/A$	$\Delta\sigma_c/A$
Pure interface	4.36	27.69	0.58	–	–
$Re^{\gamma\text{-}(Ni)}$	4.28	28.26	0.56	−0.08	0.57
$Re^{\gamma'\text{-}(Al)}$	5.55	34.79	0.59	1.19	7.10
$Re^{\gamma'\text{-}(Ni)}$	4.89	31.04	0.58	0.53	3.35
$Ru^{\gamma\text{-}(Ni)}$	4.29	28.16	0.56	−0.07	0.47
$Ru^{\gamma'\text{-}(Al)}$	5.18	33.14	0.57	0.82	5.45
$Ru^{\gamma'\text{-}(Ni)}$	4.33	27.71	0.58	−0.02	0.02

Cleavage energy per area G_c/A in J/m^2, critical stress σ_c/A in GPa, critical length l in Å, cleavage energy change $\Delta G_c/A$ in J/m^2, relative changes $\Delta\sigma_c/A$ in GPa with respect to pure interface.

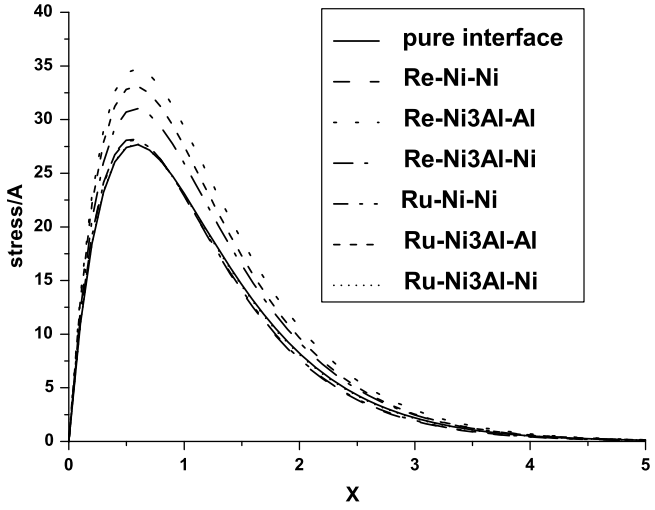

Fig. 6. The calculated stress per unit area $\sigma(x)/A$ in (J/m^3) verse the interface separation x(Å) for substitutions Re and Ru at γ-*Ni*,γ′-Al and γ′ − Ni sites.

the critical energy release rate G_d. Rice [18] pointed out that, to emitting a dislocation, it is necessary to follow the minimum-energy trajectory between the point 0 and ***b***. At some point, the energy reaches the maximum value along this path. Rice called this energy – unstable stacking fault energy, $\gamma_{\mu s}$. The emission of a dislocation is a complex process, it could be infected by many aspects, such as the geometry and the direction of the crack, and the type of the dislocation. So the relationship between G_d and the intrinsic parameters of the material is still under discussion. When a dislocation is emitted on the same plane with the crack, Rice [18] pointed out that G_d is equal to the unstable stacking fault energy $\gamma_{\mu s}$ mentioned above. $\gamma_{\mu s}$ is defined as the maximum of the generalized stacking fault energy $\gamma_{\mu s} = \max(\gamma_{GSF}(\boldsymbol{u}))$ [22,38]. $\gamma_{GSF}(\boldsymbol{u})$ is the energy needed to slip the two blocks of the material against each other in the direction ***u***.

The calculated models describe the case of a dislocation emitting on slip plane coinciding with the crack plane. In this premise, $G_d = \gamma_{\mu s}$. We define a quantity $D = G_c/G_d$, to reflect the ductile-to-brittle crossover. For ratios smaller than 1 the material is considered to be brittle.

4.1. ⟨100⟩(001) slip

Single crystal nickel-based superalloy of [001] orientation could be prepared by means of the crystal selection method [39]. (001) cleavage habit plane is the preferred slip plane as well. We first come to investigate the ⟨100⟩(001) slip. Fig. 7 gives the ⟨100⟩(001) slip with or without dopants. For the pure γ/γ′ interface, the generalized stacking fault energy $\gamma_{GSF}(\boldsymbol{u})$ increases smoothly with ***u***, and reach the maximum energy value $\gamma_{\mu s} = 1.782$ J/m^2 at 0.5***b***. By doping Re, the trend of generalized stacking fault energy γ_{GSF} curve changes greatly compared with pure interface. γ_{GSF} gets its maximum value at 0.2***b***, $\gamma_{\mu s} = 0.25$, 0.28, 0.27 J/m^2 for $Re^{\gamma\text{-}Ni}$, $Re^{\gamma'\text{-}Al}$, $Re^{\gamma'\text{-}Ni}$ substitutions, respectively. By doping Ru, the trend of generalized stacking fault energy γ_{GSF} curve is the same with doping Re. γ_{GSF} gets its maximum value at 0.2***b***, $\gamma_{\mu s} = 0.27$, 0.28, 0.27 J/m^2 for $Ru^{\gamma\text{-}Ni}$, $Ru^{\gamma'\text{-}Al}$, $Ru^{\gamma'\text{-}Ni}$ substitutions, respectively. The results are listed in Table 4. Both of doping Re and Ru reduce $\gamma_{\mu s}$ significantly. This trend increase the ductility of ⟨100⟩(001) slip. The largest D value listed in Table 4 is 19.95 with respect to $Re^{\gamma'\text{-}Al}$ substitution.

4.2. ⟨110⟩(001) slip

⟨110⟩ and ⟨100⟩ are two different low index slip directions. Fig. 7 gives the generalized stacking fault energy curve of ⟨110⟩(001) slip. The $\gamma_{\mu s}$ and D value are listed in Table 4. For pure interface, the value of γ_{GSF} increases with ***u***, when $\boldsymbol{u} < 0.25\boldsymbol{b}$. Then reaches its maximum value $\gamma_{\mu s} = 1.12$ J/m^2 at 0.25***b***. Finally, the value of γ_{GSF} decrease with ***u***. By doping Re, $\gamma_{\mu s}$ is significantly reduced. It is 0.13, 0.134, 0.124 J/m^2 for $Re^{\gamma\text{-}Ni}$, $Re^{\gamma'\text{-}Al}$, and $Re^{\gamma'\text{-}Ni}$ substitutions, respectively. While in the case of doping Ru, it is 0.122, 0.133, 0.127 J/m^2 for $Ru^{\gamma\text{-}Ni}$, $Ru^{\gamma'\text{-}Al}$, and $Ru^{\gamma'\text{-}Ni}$ substitutions, respectively. The largest D value listed in Table 5 is 41.54 with respect to $Re^{\gamma'\text{-}Al}$ substitution. Doping Re and Ru could increase the ductility of (001) interface. $Re^{\gamma'\text{-}Al}$ substitution is the most favored case in ⟨110⟩(001) slip.

4.3. Comparison between ⟨100⟩(001) and ⟨110⟩(001) slip

For pure interface, the value D for ⟨100⟩(001) and ⟨110⟩(001) slip is 2.445 and 3.875, respectively. This suggest that slipping in the ⟨110⟩ direction is more easier than that in ⟨100⟩ direction, and this conclusion is the same with experiment results [39]. By doping Re and Ru, $\gamma_{\mu s}$ is significantly reduced, but $\gamma_{\mu s}$ for ⟨110⟩ slip is smaller than that of ⟨100⟩ slip. From D values listed in Table 4, we can get a conclusion that ⟨110⟩ slip is more favorable than ⟨100⟩ slip.

Table 5 lists interface separations of the different substitutions. Doping Re or Ru at γ′-Al site increase the coherent strength of γ/γ′ interface, and the bond length is shorter than other cases. Doping

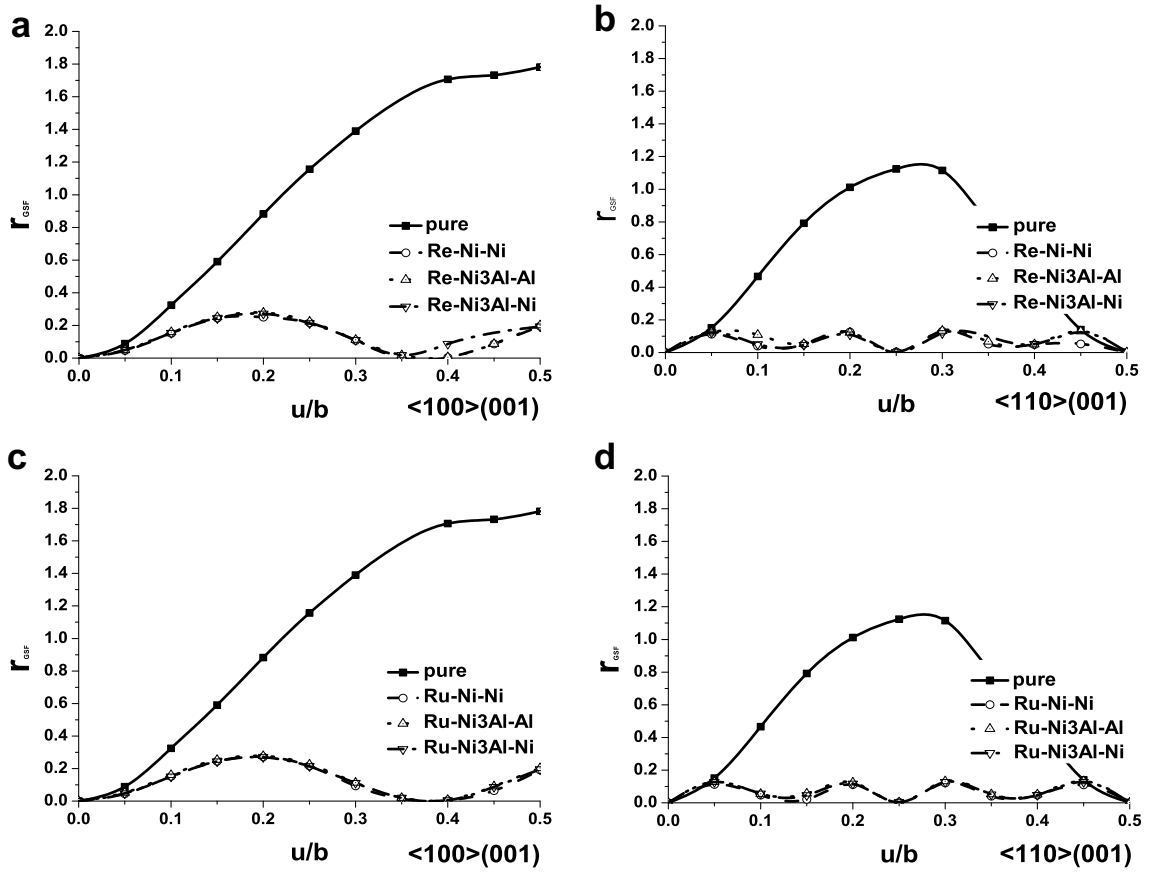

Fig. 7. The generalized stacking fault energies (γ_{GSF} in J/m^2) curve verse the slipping displacement ($\boldsymbol{u}/b$) of γ/γ' interface doped with Re and Ru. (a) $\langle 100\rangle(001)$ slip for the pure and Re substitution interface; (b) $\langle 110\rangle(001)$ slip for the pure and Re substitution interface; (c) $\langle 100\rangle(001)$ slip for the pure and Ru substitution interface; (d) $\langle 110\rangle(001)$ slip for the pure and Ru substitution interface.

Table 4
The calculated quantities of the pure γ/γ' interface and doped interface

	$\gamma\mu_s$		D	
	$\langle 100\rangle(001)$	$\langle 110\rangle(001)$	$\langle 100\rangle(001)$	$\langle 110\rangle(001)$
Pure interface	1.782	1.125	2.445	3.875
$Re^{\gamma\text{-(Ni)}}$	0.250	0.130	17.085	32.887
$Re^{\gamma'\text{-(Al)}}$	0.278	0.134	19.946	41.540
$Re^{\gamma'\text{-(Ni)}}$	0.272	0.124	17.998	39.455
$Ru^{\gamma\text{-(Ni)}}$	0.272	0.122	15.808	35.226
$Ru^{\gamma'\text{-(Al)}}$	0.278	0.133	18.650	38.988
$Ru^{\gamma'\text{-(Ni)}}$	0.269	0.127	16.084	34.015

$\gamma\mu_s$ in J/m^2, and G_c/G_d.

Table 5
The interface separation (Å) of different substitutions

Pure interface	$Re^{\gamma\text{-(Ni)}}$	$Re^{\gamma'\text{-(Al)}}$	$Re^{\gamma'\text{-(Ni)}}$	$Ru^{\gamma\text{-(Ni)}}$	$Ru^{\gamma'\text{-(Al)}}$	$Ru^{\gamma'\text{-(Ni)}}$
1.77	1.85	1.78	1.80	1.82	1.77	1.80

Re and Ru could reduce $\gamma\mu_s$ significantly, and $\gamma\mu_s$ is not sensitive to doping site. So the slip behavior does not sensitive to doping site, but relies on the dopants and slip directions. On the other hand, G_c is sensitive to the dopants and doping sites.

5. Conclusion

In this work, we have investigate the γ/γ' interface doped with Re and Ru. The site preference, cleavage properties and slip properties are calculated within the framework of density functional theory. It is find that both Re and Ru tend to place at the γ'-Al site at the interface. And through doping Re and Ru, the critical cleavage energies have been increased, and the $\gamma\mu_s$ has been reduced. This means, by substitutions with Re and Ru, the ductility of γ/γ' interface is improved.

Acknowledgement

This research was supported by 973 Project from the Ministry of Science and Technology of China (Grant No. 2006CB605102).

References

[1] A.M. Huntz, B. Lefevre, F. Cassino, Mater. Sci. Eng. A 290 (2000) 190.
[2] W. Betteridge, in: Nickel and Its Alloys, Macdonald and Evans, Estover, United Kingdom, 1977, p. 124.
[3] N.S. Stoloff, C.T. Liu, S.C. Deevi, Intermetallics 8 (2000) 1313.
[4] T. Hirano, Fracture Strength of Grain Boundaries in Ni_3Al, presented at the University of Saarland, Saarbrucken, Germany, December 8, 2000.
[5] S.X. McFadden, R.S. Mishra, R.Z. Valiev, A.P. Zhilyaev, A.K. Mukherjee, Nature 398 (1999) 684.
[6] M. Yamaguchi, H. Inui, K. Ito, Acta Mater. 48 (2000) 307.
[7] G.R. Odette, B.L. Chao, J.W. Sheckherd, G.E. Lucas, Acta Metall. Mater. 40 (1992) 2381.
[8] J. Heathcote, G.R. Odette, G.E. Lucas, Acta Mater. 44 (1996) 4289.
[9] G.L. Erickson, A New, Third Generation, Single-Crystal, Casting Superalloy, JOM, TMS, Warrendale, PA, 47, No. 4, April, 1995, p. 36.
[10] K.S. O'Hara, W.S. Walston, E.W. Ross, R. Darolia: U.S. Patent, No. 5,482,789, 1996.
[11] Q. Feng, L.J. Carroll, T.M. Pollock, Metall. Mater. Trans. A 37A (2006) 1949.
[12] M. Durand-Charee, The Microstructure of Superalloys, Gordon and Breach Science Publishers, Canada, 1997, p. 60.

[13] G.E. Fuchs, Mater. Sci. Eng. A 300 (2001) 52.
[14] Atsushi Sato, Hiroshi Harada, Tadaharu Yokokawa, Takao Murakumo, Yutaka Koizumi, Toshiharu Kobayashi, Hachiro Imai, doi:10.1016/j.scriptamat.2006.01.003.
[15] A.P. Ofori, C.J. Rossouw, C.J. Humphreys, Acta Mater. 53 (2005) 97.
[16] H. Murakami, T. Honma, Y. Koizumi, H. Harada, in: T.M. Pollock, R.D. Kissinger, R.R. Bowman, K.A. Green, M. McLean, S.L. Olson, J.J. Schirra (Eds.), Proceedings of the Nineth International Symposium on Superalloys, TMS, Seven Springs (PA), 2000, p. 747.
[17] J.R. Rice, R. Thomson, Philos. Mag. 29 (1974) 73.
[18] J.R. Rice, J. Mech. Phys. Solids 40 (1992) 239.
[19] C.L. Fu, J. Mater. Res. 5 (1990) 971.
[20] M.H. Yoo, C.L. Fu, Mater. Sci. Eng. A 153 (1992) 470.
[21] P. Lazar, R. Podloucky, W. Wolf, Appl. Phys. Lett. 87 (2005) 261910.
[22] V. Vitek, Philos. Mag. 18 (1968) 773.
[23] U.V. Waghmare, V. Bulatov, E. Kaxiras, M.S. Duesbery, Mater. Sci. Eng. A 261 (1999) 147.
[24] P. Lazar, R. Podloucky, Phys. Rev. B 73 (2006) 104114.
[25] N.I. Medvedeva, Y.N. Gornostyrev, O.Y. Kontsevoi, A.J. Freeman, Acta Mater. 52 (2004) 675.
[26] G. Kresse, J. Hafner, Phys. Rev. B 47 (1993) R558.
[27] G. Kresse, J. Furthmller, Comput. Mater. Sci. 6 (1996) 15.
[28] J.P. Perdew, Y. Wang, Phys. Rev. B 45 (1992) 13244.
[29] P.E. Blöchl, Phys. Rev. B 50 (1994) 17953.
[30] Y. Wang, Z.-K. Liu, L.-Q. Chen, Acta Mater. 52 (2004) 2665.
[31] Y. Mishin, Acta Mater. 52 (2004) 1451.
[32] Available from: http://www.webelements.com/.
[33] A.B. Kamara, A.J. Ardell, C.N.J. Wagner, Metall. Mater. Trans. A 27 (1996) 2888.
[34] Y.M. Sun, G.E. Beltz, J.R. Rice, Mater. Sci. Eng. A 170 (1993) 67.
[35] J. Hartford, B. von Sydow, G. Wahnström, B.I. Lundqvist, Phys. Rev. B 58 (1998) 2487.
[36] J.H. Rose, J.R. Smith, J. Ferrante, Phys. Rev. B 28 (1983) 1835.
[37] C.E. Inglis, Trans. Inst. Naval Arch. 55 (1913) 219.
[38] J.W. Christian, V. Vitek, Rep. Prog. Phys. 33 (1970) 307.
[39] Sugui Tian, Xingfu Yu, Jinghong Yang, Nairen Zhao, Yongbo Xu, Zhuangqi Hu, Mater. Sci. Eng. A 379 (2004) 141.